ELSEVIER

Sensors and Actuators A 88 (2001) 93–103

SENSORS AND ACTUATORS A PHYSICAL

www.elsevier.nl/locate/sna

Feasibility study on a contact-less direct thermal printing with electrothermal SPICE simulation

Yeong-Maw Chen*, Jin-Shown Shie

Institute of Electro-Optical Engineering, National Chiao Tung University, 1001 Ta Hsueh Road, Hsinchu, Taiwan, ROC

Accepted 29 August 2000

Abstract

A new concept for making contact-less direct thermal printing for facsimile is proposed and evaluated in this article. The concept is based on the fact that air molecules can be a good thermal conduction medium capable of transferring the heat efficiently from a micro-heater to a thermal marking paper, if both in close proximity. The micro-heater can be made of single-crystal silicon by micromachining technology, hence the associated CMOS driving circuits can be fabricated monolithically with the heater to exempt from the tedious work of numerous wire bonding. An illustrative device of integrated micro-heater array in 200 dpi resolution has been fabricated, characterized and evaluated for the new printing application. A thermal model of the device has also been set up and studied of its dynamic behaviors using the existing electrothermal SPICE package. The result of simulations indicates that efficient energy transfer of more than 40%, much better than the conventional performance, can be achieved with a practical 1 μm air gap. This and other additional advantages described in the article indicates that, in principle, the contact-less direct thermal printing is feasible and the monolithic silicon micro-heater array can be an excellent device for this application. © 2001 Elsevier Science B.V. All rights reserved.

Keywords: Thermal printing head; Facsimile; Direct thermal printing; Gaseous heat conduction; Micro-heater; Electrothermal SPICE

1. Introduction

The technology of direct thermal printing (DTP) has been adopted for decades [1–3]. Comparing to other mature technologies, it is still considered to be the most convenient and cost-effective way of printing a facsimile message and others, such as cashier data [1].

A direct thermal printer has to print the demanded information onto a special thermal marking paper by physical contact with certain heating elements at the corresponding paper locations whereupon the thermo-chemical blacken reaction in the coating material is induced [2]. In order to cause such a reaction, a proper thermal power must be generated from a resistive heating element and transferred efficiently by all means onto the paper surface. Since the thermal transferring process is generally comparatively slow, a single heating element with the conventional raster scan mechanism, such as that used in the current ink jet printing, will not be faster enough to provide satisfactory printing speed for practical applications, like A4-size printing. Instead, a module which comprises a long linear array of heating elements with an electronically scan-and-drive IC must be adopted, so that a line of data can be printed out simultaneously, which naturally gains the speed required. The module performing such an electro-mechanical hybrid scan is generally named as thermal printing head (TPH) [3], which is the heart of the current direct thermal printers.

At present, there are two ways of making a TPH resistor array, the thick-film and thin-film methods [3]. The former type has the advantages of high production throughput and cost-effective, but it is unfavorable in power consumption and resistance uniformity compared to the latter type. As shown in Fig. 1, all current direct thermal printers require physical sliding between the TPH heater and the thermal marking paper. This sliding causes inevitable wearing on the heater part, therefore, a wear-resist glaze must be applied over the resistor surfaces to ensure the reliability. However, the glaze, which is not a thermally conductive material, impedes the heat flowing to the paper and causes more heat loss unfavorably to the opposite TPH substrate usually a printed circuit board (PCB) material. The shortcoming not only reduces the efficiency of the printing power but also increases the heater and substrate temperatures, making the thermal management crucial in the printer system design. This also explains why the thin-film-type TPH is better, since a thinner resistor requires only a thinner glaze, the

* Corresponding author. Tel.: +886-3-489-1671 (H)/+886-3-445-3787 (O); fax: +886-3-471-2306.
E-mail address: ymcmail@seed.net.tw (Y.-M. Chen).

0924-4247/01/$ – see front matter © 2001 Elsevier Science B.V. All rights reserved.
PII: S0924-4247(00)00497-0

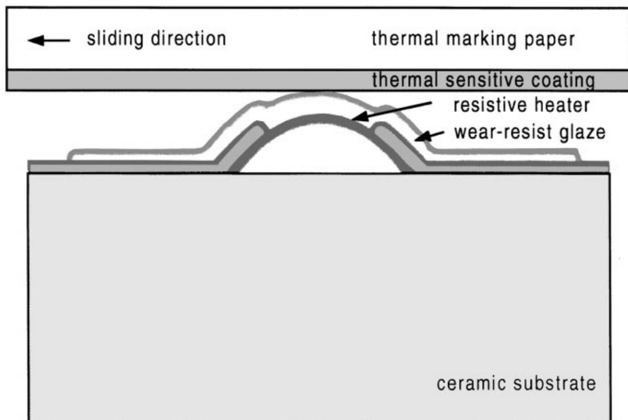

Fig. 1. Structure of the conventional direct thermal printing.

thermal resistance to the paper thus can be reduced to achieve better thermal efficiency. In a present commercial thin-film TPH of 200 dpi (dot per inch) resolution and 10 ms/line speed, a small heating energy of 0.4 mJ/dot is enough to heat the thermal marking paper up to the blacken temperature which is generally defined between 70 and 150°C [2]. In such case, the heat transfer efficiency estimated is ~20% with the maximum PCB substrate temperature being kept within a safety, but not satisfactory, 70°C during the operation [3].

Although this kind of contact-type direct thermal printer has been commercialized for quite a period, research on designing better TPH with improved performance should be still the industrial goal [3]. In this article, the authors try to explore a new non-contact DTP method capable of avoiding the shortcomings in the conventional TPH. Besides that, the resistor elements can be micro-fabricated on the same silicon wafer together with the driving circuits to avoid the numerous wires bonding between the individual resistors and the multiplexing IC. The details will be described in the following content.

2. The basic principle

The method proposed in this report of achieving contactless DTP is based on the fact that air molecules can act as an efficient heat transfer medium between a pair of heat source and sink in close proximity. Hence the molecules in the shallow gap experience high collision rates with them. More details are described below.

Fig. 2 depicts two plates, having a temperature difference ΔT, face each other with a shallow spacing s. In our case, the hotter is assumed to be the heating element, while the colder is the paper to be printed. The molecules bounce back and forth between the two plates will carry simultaneously the differential thermal energy from the hotter plate and dump to the colder one. According to the gas kinematics, the collision is ballistic at low gas pressure, while at high pressure it becomes diffusive due to shortening of the mean free path. In early Smoluchowski's and the related analyses [4–6], the gaseous thermal conductance (in W/°C) at pressure P can be expressed by

$$G_g = C_1 A\sqrt{\frac{273.2}{T}} \times \frac{PP_t}{P + P_t}\ (\mathrm{W/^\circ C}) \tag{1}$$

with the transition pressure (in Torr)

$$P_t = C_2 \frac{kT}{\delta^2} \times \frac{1}{s}\ (\mathrm{Torr}) \tag{2}$$

Here both C_1 and C_2 are functions of various physical parameters in gas kinetics theory [5], δ and kT are the molecular diameter and Boltzmannian thermal energy, respectively, and A is the heat dissipation area.

At high pressure condition where $P \gg P_t$

$$G_g \approx C_1 A\sqrt{\frac{273.2}{T}} P_t = C_1 A\sqrt{\frac{273.2}{T}} \times C_2 \frac{kT}{\delta^2} \times \frac{1}{s} = K_g \frac{A}{s} \tag{3}$$

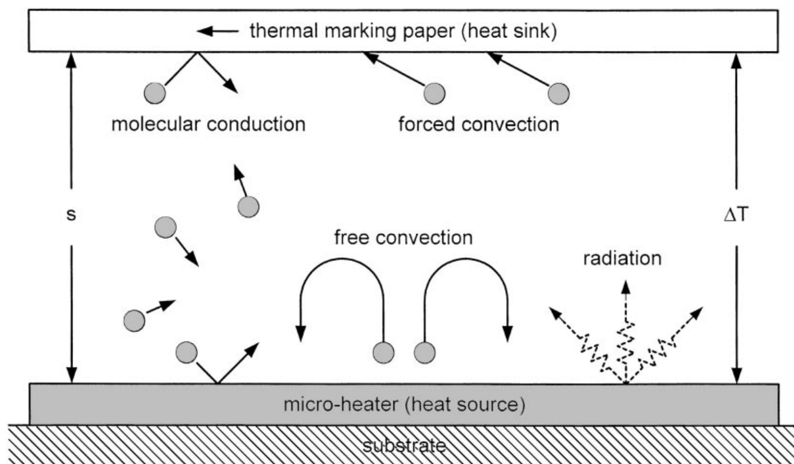

Fig. 2. A schematic representation of the various heat-transfer mechanisms between a micro-heater to a thermal marking paper in close proximity.

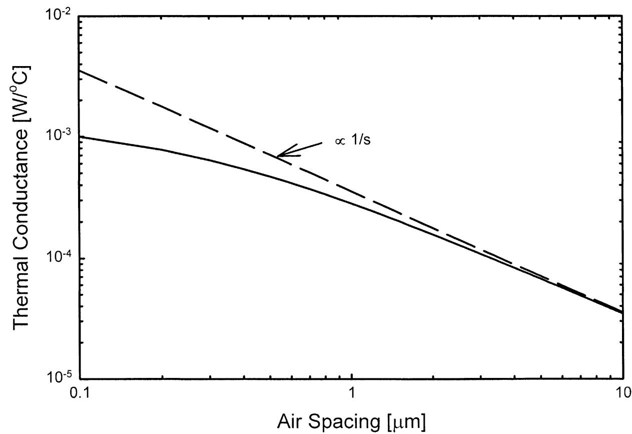

Fig. 3. Effect of air gap on gaseous thermal conductance at standard state (1 atm, 0°C). Notice that the thermal conductance mechanism starts to be gap-limited scattering below few micron spacing.

Table 1
Thermal conductance of various mechanisms between two plates

Thermal conductance (mW/°C)	Paremeters
Gaseous conductance	
471.0	$s = 0.5$ μm
283.0	$s = 1.0$ μm
67.6	$s = 5.0$ μm
34.7	$s = 10.0$ μm
Free convection[a]	
7.0	Standard-state air
Forced convection[b]	
1.4	Speed = 12 mm/s
13.6	Speed = 1200 mm/s
Radiation[c] (ambient $T = 27$°C)	
0.2	Heater $T_h = 200$°C
0.6	Heater $T_h = 500$°C

[a] [7].
[b] [8].
[c] [9].

Hence the thermal conductance is inversely proportional to the spacing (s) between the plates. This implies that, in our application, the printing device must be kept close enough to the printed paper during operation so that sufficient heat can flow through the gas. One also notes that the thermal conductivity K_g in Eq. (3) is weakly temperature-dependent around the room temperature. For air at the standard state, K_g is equal to 2.47×10^{-4} W/cm °C based on the theory [5]. According to Eq. (2), when the spacing s is reduced, P_t becomes inversely larger and comparable to the pressure P, the thermal conduction then depends less on the spacing. The behavior is depicted in Fig. 3 in accordance with Eqs. (1) and (2), where one can observe the slower rising of the air thermal conductance when the spacing is in 1 μm range.

As depicted in Fig. 2, the energy in the hot plate can also dissipate by other loss mechanisms. A major portion of this heat goes directly to the substrate holding the heater by solid conduction. This loss is totally useless to our purpose. Also, a certain portion of the heat is lost to the air by convection mechanisms, either directionally biased by the wind velocity as forced convection or by the fluid density as free convection [7,8]. Both mechanisms are difficult to control and should be reduced to the minimum in our purpose. There is another mechanism due to the net thermal radiation from the heater to the surroundings, however, only a part of this radiation is projected usefully to the paper surface, while the rest is wasted. Table 1 lists the numerical calculation on the relative magnitudes of these mechanisms, except the solid loss to the substrate, which depends very much on the device structure and will be treated separately later on.

One notes from the Table 1 that, even in 5 μm spacing, the dominating molecular thermal conductance is still having an order of magnitude larger than the free convection, not to mention the rest. This suggests that micron spacing between a paper and a heating element indeed is necessary for the air molecules to play the main role in directing the heat to the thermal marking paper. The value of air thermal conductivity (2.47×10^{-4} W/cm °C) is only ~1/60 of that of SiO_2 glaze (0.014 W/cm°C) [10], nevertheless, the glaze in the conventional TPH is thicker (~7 μm) and its thermal capacitance, as a solid, is also four-orders of magnitude larger than the air thermal capacitance [5,10]. Consequently, the thermal response time in the conventional TPH is a hundred times slower than our proposed device using air as the conduction medium. This fact will be revealed later on in our simulation study.

The thermal loss through device solid structure usually is the largest loss factor in the conventional TPHs. It must be minimized to a practical tolerance by careful consideration, otherwise the substrate might be overheated into an unsafe situation. A special device configuration with sufficient thermal isolation to the heater must be designed and fabricated to satisfy the application demand. In the present proposed method, this can be easily made by silicon micromachining technique as will be described below.

3. The device microfabrication and the performance

Before entering the simulation, fabrication of a microheater array and the driver IC in a monolithic silicon chip will be described first, in order to understand the advantages of the new TPH device. The process steps are depicted in Fig. 4a (1 0 0) silicon wafer is cleaned, pre-oxidized and deposited with LPCVD nitride. The passivated surface is photolithographically patterned and etched on the field oxide area and border of the micro-heater to be fabricated. In this step, not only the passivation layers are etched out, the silicon exposed is also etched back to a pre-designed depth (Fig. 4a), hence in the next selective oxidation the etched space can be filled up by oxide nearly to the original silicon level (planerization). After the nitride passivation is stripped off (Fig. 4b), gate thin oxide is grown and polysilicon is deposited and patterned by lithographic process, then

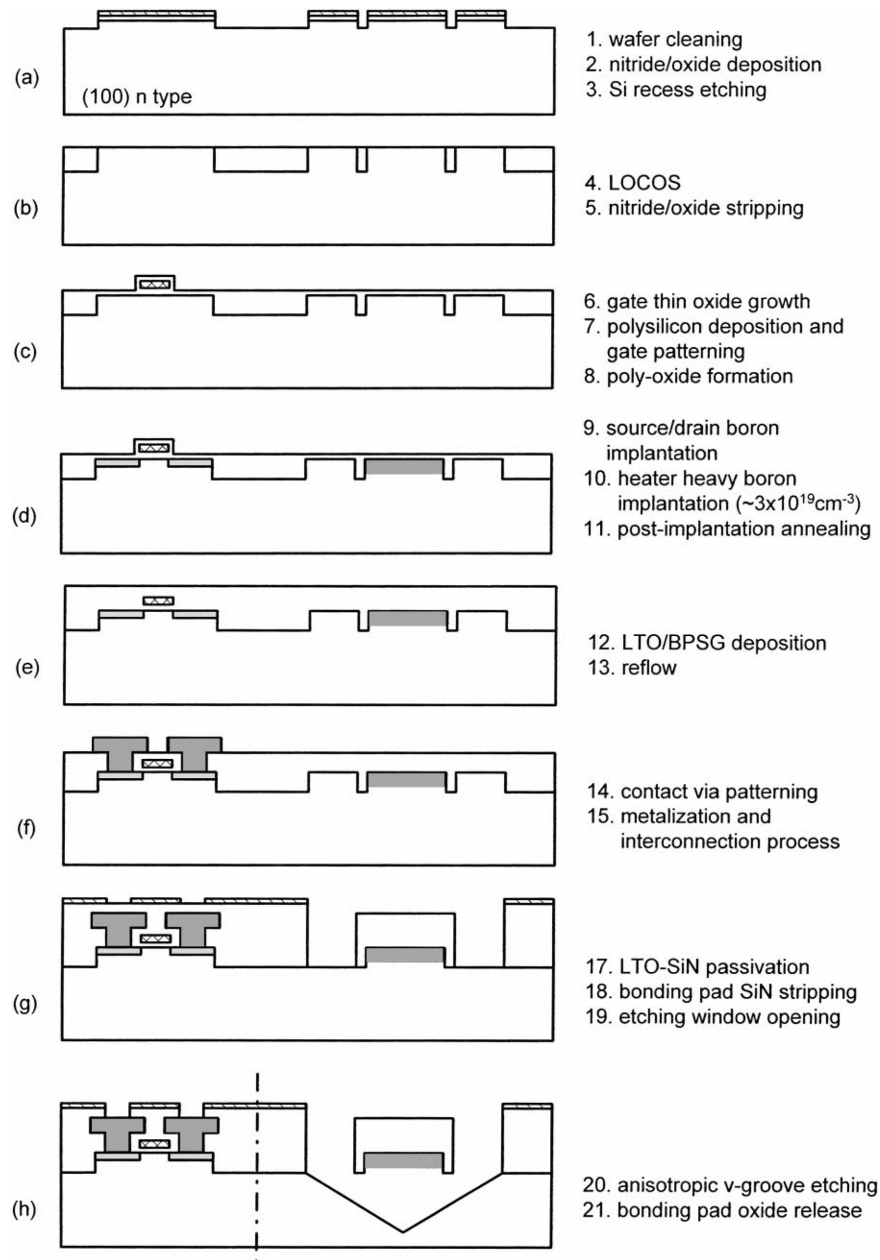

Fig. 4. Fabrication processes of the monolithic thermal printing device proposed in this study.

proceeded to polyoxide formation (Fig. 4c). After the self-aligned, shallow source/drain boron implantation is performed on the MOS switch and micro-heater area, an additional deeper, heavily dosed boron ($\sim 3 \times 10^{19}$ cm^{-3}, 120 keV) implantation is applied subsequently on the micro-heater area alone. This extra step provides the future heater thickness and resistance can be tuned according to the demand (Fig. 4d). Although it is not regular in the standard CMOS processes by all foundries, nevertheless it is tolerable and cost-effective. After finishing post-implant annealing, CVD oxide and then BPSG are deposited and proceeded to reflow step for planarization (Fig. 4e). Sequentially, the standard processes for contact-via patterning, aluminum metallization, and LTO and PECVD nitride passivations are followed (Fig. 4f). Then, the nitride on the bonding-pad and micro-heater areas are stripped off by selective dry etching, leaving a thin layer of LTO on the aluminum pad area for protection from the later anisotropic etching (Fig. 4g). Finally, a trench window is made lithographically around the heavily doped B^{++} bridge area allowing for the v-groove etching to proceed, which renders the B^{++}-doped micro-heater floating in the end. When the micromachining step is finished, the wafer is subjected to light (several seconds) wet etching in BOE solution to remove the remaining LTO oxide previous left over the aluminum pad (Fig. 4h).

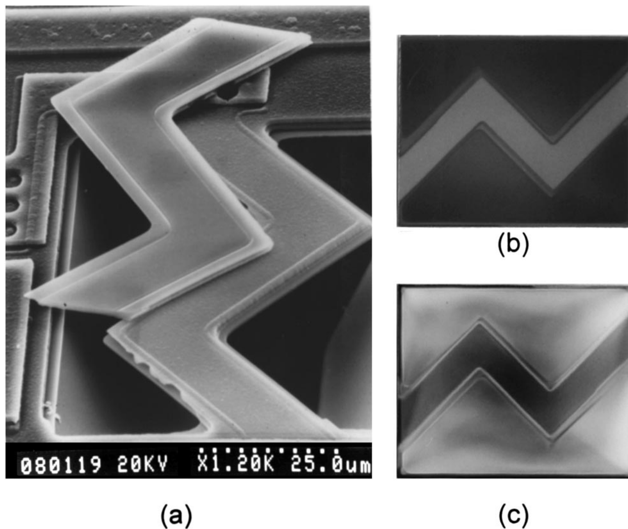

Fig. 5. (a) A SEM picture of the fabricated micro-heater. Notice that the border of glass on the broken bottom–up element and the clear-cut edge of the remained silicon heater; (b) and (c) denotes photographs taken by Romenski microscope in dark and bright fields. The flatness of the bridge can be realized by the uniform color of the pictures. Also the protective LOCOS side wall around the silicon heater is also observable.

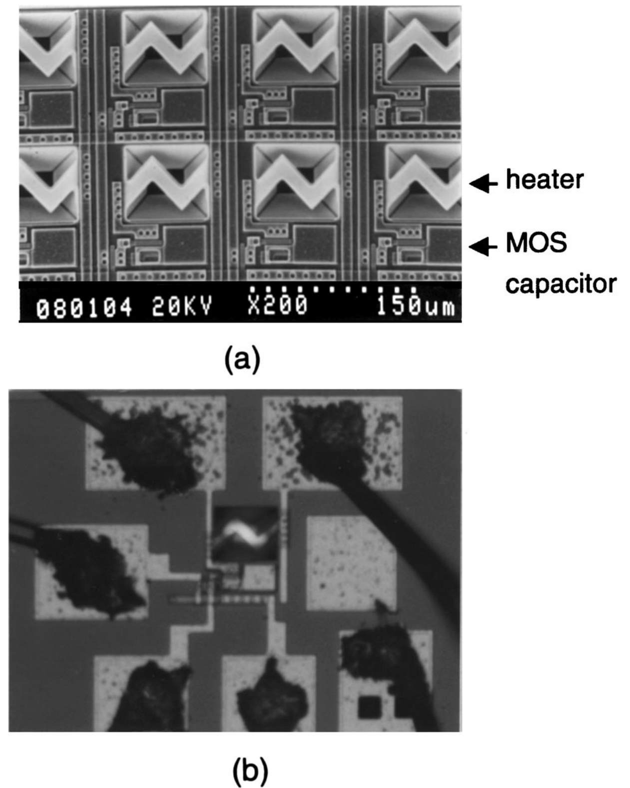

Fig. 6. (a) SEM picture of a fabricated micro-heater array with the associated signal switching-and-holding circuit; (b) a test dot in active operation.

One should be aware that all MOS devices are protected by passivations and isolated from v-groove regions during the anisotropic etching, while the micro-heater is protected by oxides on the top and rim, which is defined by lithographic step 19 of Fig. 4g. Meanwhile, the heavy B^{++} doping in silicon material stops the etching from bottom [11]. This is evident by the SEM picture of a broken bottom–up element in Fig. 5a. The LOCOS border around the floating resistors not only guards them from irregular etching on the resistor boundary so that the resultant bridge pattern can be more uniform in all resistor elements, but also that the device is structurally stronger with the border oxide.

One should also note that, in the final device structure, the demanded shallow spacing, from the thermal marking paper pressed on the highest nitride layer to floating micro-heater, can be fabricated accurately simply by adjusting the processed nitride thickness. The flatness of the resistor beneath the glass coat is also observable under a Romenski microscope in dark and bright fields as that shown in Fig. 5b and c. This indicates that the shallow gap between the micro-heater and the printed paper can be kept in controlled accuracy.

Fig. 6a shows the SEM picture of a part of the fabricated device, where a switch MOS device, a charge holding capacitor and the B^{++}-doped floating resistor are assorted in each pixel area. The micro-fabricated floating structure renders the resistive heater thermally isolated, hence a minute Joule heating derived from the external circuit can rise the element to a temperature sufficient high for thermal printing need. Notice that two lines of micro-heaters are made so that one can be the redundancy of the other to ensure better yield. Fig. 6b demonstrates a tested dot in active operation where the floating resistor is burned into red hot.

The equivalent circuit of the monolithic resistor array in Fig. 6a is depicted in Fig. 7. Here the micro-heater is placed in between the MOS drain and the ground. This circuit configuration plays a linearization function due to the effect of negative feedback between the device input (gate signal) and the output (heater temperature), thus the heater temperature can be better controlled electronically. On the other hand, if the resistor is placed at the source end without feedback, the heater temperature will be highly non-linear in relating to the gate input, because of the strongly temperature-dependent nature of semiconductor resistivity. This is revealed in Fig. 8 by the characteristic measurements of the tested dot. One observes a much better linearly ramping in the feedback case compared to the non-feedback situation. Therefore, the heater temperature can be easily controlled by the external electronics. In the experiment, a PbSe infrared detector is used to estimate the temperature pyrometrically according to the Stefan–Boltzmann T^4 law [9].

4. The simulation

The printing configuration related to the fabricated device and the thermal marking paper is depicted in Fig. 9. The

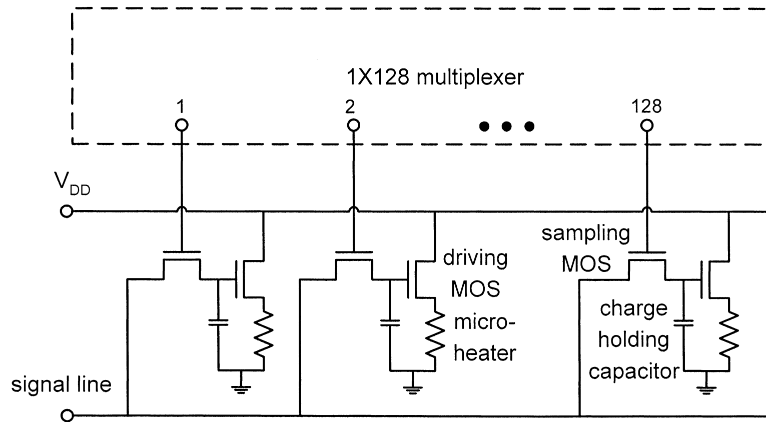

Fig. 7. The circuit configuration of the monolithic micro-heater array. Each dot is associated with a sampling MOS, a signal-holding capacitor, a driver MOS, and a floating silicon resistor.

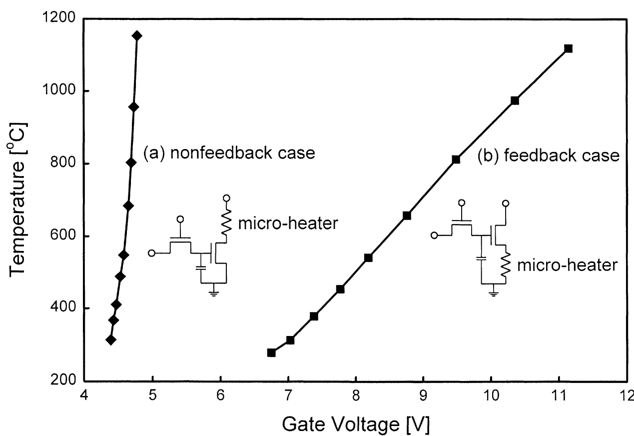

Fig. 8. The pyrometrically measured heater temperatures under various applied gate voltages without (curve a) and with (curve b) negative feedback circuit. Notice that the better linearity of the heater temperature with respect to the input gate voltage in feedback case.

paper should be placed in intimate contact with the nitride passivation on the device surface, thus holding a fabricated spacing to the micro-heater surface when thermal printing is proceeded. Since the air gap in v-groove region is not flat, an equivalent surface below the heater shall be assumed for simplicity of analysis. This is denoted by the dotted line aa′ in Fig. 9. Calculation of this equivalent spacing is based on the integration of Eqs. (1) and (2) in differential forms. This value has been evaluated before by Weng and Shie [12] with an empirical rule of ∼18% of the v-groove width.

The heat loss behavior of such an configuration can be studied by converting it to an equivalent electrothermal SPICE model [13], which takes the advantage of utilizing the existing SPICE package for simulation. This model has been used successfully by many researchers in analyzing thermal-type micro-sensors [13–16] and micro-heaters [17]. The equivalent electrothermal circuit of the present device is

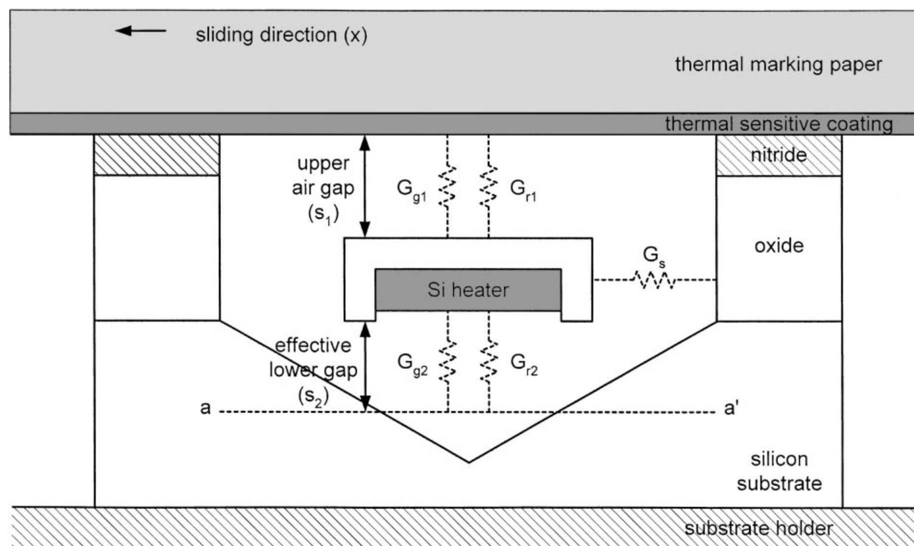

Fig. 9. The schematic cross-sectional view of the present contact-less, thermal printing device where the thermal marking paper is pressed on the nitride passivation surface. Heat-loss paths are also indicated in the figure by the broken symbols. The effective gap of v-groove below the heating element is represented by aa′ line.

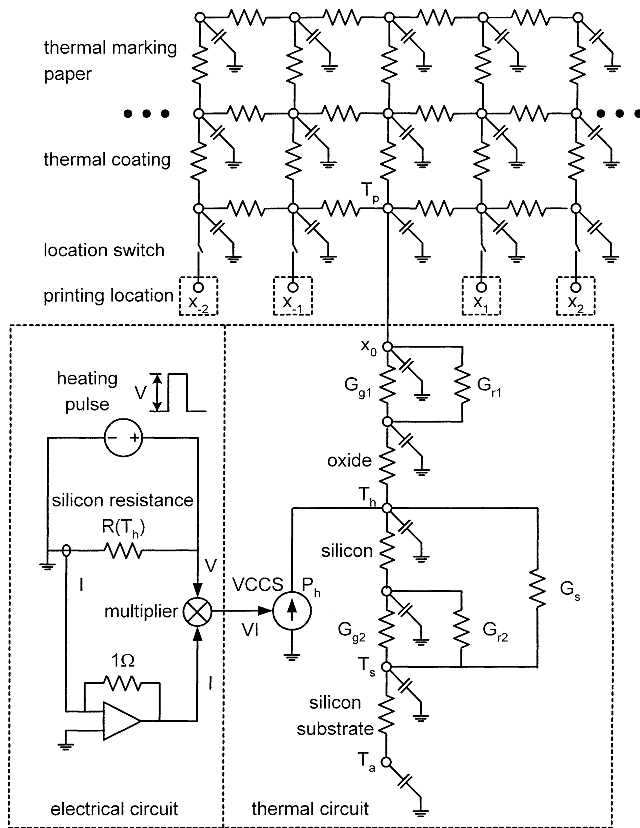

Fig. 10. Analogy thermal circuit of the present thermal printing device. In thermal circuit, a resistor represents a thermal resistance along a heat-loss path, and a capacitor stands for an associated thermal mass. The ground is equivalent to the ambient temperature, 27°C is assumed in the study.

summarized in Fig. 10. In the upper part of the figure, the periodic network represents different printing locations on a thermal marking paper along its moving direction. The network includes both the vertical and lateral heat spreading on paper. The position x_0 is the point where the printing is under execution by closing the switch. The details of the contact-less thermally printing pixel is depicted by the enlarged box at x_0, where the left part is the electrical circuit while the right part is the thermal circuits. In the thermal circuit, a resistance symbol represents a thermal conduction path, and a capacitance symbol stands for heat capacity of the related material. In the electrical circuit, the heating pulse voltage V is applied on the silicon micro-heater, $R(T_h)$, and its Joule's heat is obtained by the product of I and V across the resistor, and represented by an equivalent output voltage at multiplier. The voltage is then fed to a voltage-controlled current source (VCCS) to produce the heat flux P_h in the right part for thermal simulation. Table 2 summarizes all the parameters in the diagram related to the present simulation study described below.

The execution time marking each dot, t_p, is determined by the printing speed, which can be expressed by

$$t_p{}^{-1} = \frac{(\text{ppm})}{60} \times L(\text{dpi}) \tag{4}$$

with (ppm) the page per minute, L the paper length. Accordingly, to an A4-size paper with 4 ppm printing speed, the execution time at each dot is approximately 10 ms [3]. In conventional TPHs, the heating resistors are lumped with their surroundings, the substrate and upper glaze, which results in an unfavorable large thermal mass, thus long thermal time delay, consequently, only a small fraction of the execution period t_p is allowed for each heater being activated. Since the energy demanded by the paper for blackening is a fixed value, a shorter activation means a higher power is necessary, therefore, the temperatures of the heaters and entire body will be also higher during operation. The effect produces heavy load on thermal management of the TPH module. In our micromachined device, the thermal time constant is very small due to the tiny thermal mass of the heater and the air in the gap, the heating duty cycle can be much longer than that of the conventional TPH, hence the power or temperature loading is reduced accordingly.

Fig. 11 depicts a simulated example according to the above model. One notes that the very dynamic rising and falling (~0.1 ms) of the heater temperature in comparing with that reported by D.J. Sanders (~1 ms) [18]. A much longer heating time (t_d) of 9 ms is allowable to the present device rather than 2 ms in general. The heating causes the paper's surface temperature rising and entering the

Table 2
Material and thermal parameters for simulation contact-less thermal printing

Layer	Thermal conductivity (W/cm °C)	Density (g/cm^3)	Specific heat (J/g °C)	Thickness (μm)	Thermal resistance (10^3 °C/W)	Heat capacitance (μJ/°C)
Thermal marking (paper)	0.00167	0.80	1.875	100	41.6	1.08
Paper[a] (coating)	0.00390	1.00	15.5	5	0.890	1.64
Upper air gap[b]	0.000197	0.00116	1.007	1	3.53	0.558
Heater[c] (oxide)	0.0138	2.22	0.745	0.3	0.0151	0.00357
(Si heater)	1.48	2.33	0.712	0.3	0.000141	0.00715
Effective lower air gap[b]	0.000244	0.00116	1.007	22	62.6	0.00377
Si substrate[c]	1.48	2.33	0.712	250	0.117	2.99

[a] [18].
[b] [5,10].
[c] [10].

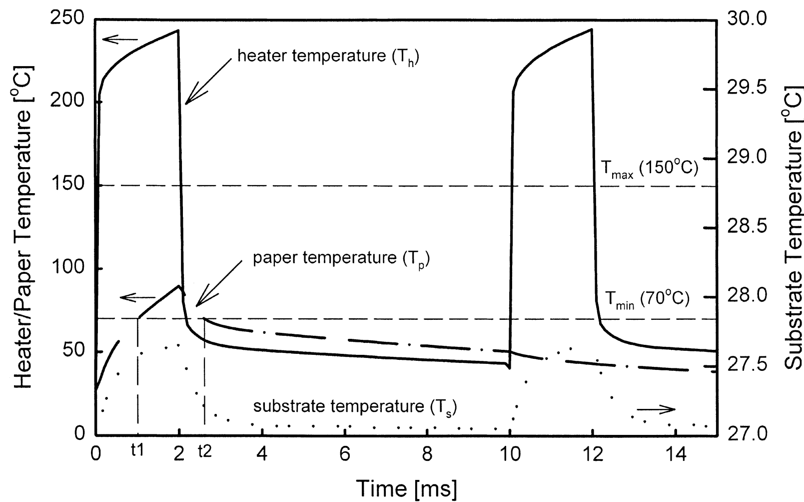

Fig. 11. The simulated time response of a 200 dpi heating element, with heating duty time t_d=2 ms, air gap s_1=1 μm, and lead solid conductance G_s=10^5 W/°C.

blackening temperature between 70 and 150°C as that shown in the figure, where the active period (from *t*1 to *t*2) in the temperature range lasts for 1.6 ms. Meanwhile, the maximum silicon substrate temperature is only slightly increased from the original 27 to 27.6°C. This is due to the excellent thermal isolation provided by the micromachined bridge structure, by which the power lost to the thermally conductive silicon substrate can be reduced drastically.

The heating energy per dot as well as other performances are systematically studied and summarized in Fig. 12. One observes the heating efficiency approaches a saturation value of ~45% when the energy is over 0.4 mJ/dot. However, energy over this value is not suitable since the paper temperature over the limited maximum of 150°C and the blackening effect will be fading out. But if the average heating temperature on the paper is restricted at the middle at 110°C, then 40% efficiency is still available. This efficiency is still considerably larger than the 20% performance of the present commercial TPH as mentioned before. Meanwhile, the heater's peak temperature is only ~300°C, which is much lower than that the present micro-heater can achieve as that depicted in Fig. 8. Hence, we can conclude that using the micro-fabricated silicon heater for direct thermal printing is feasible.

Despite good thermal isolation of the micromachined device, the solid thermal conduction along the bridge is still the major factor of power loss, therefore, good structural layout having sufficient lead thermal resistance without suffering mechanical stiffness is necessary. Fig. 13 reveals this effect: a larger heating power is required for smaller solid thermal resistance. Notice that, at 12 V supply voltage, a 30% efficiency demands only a loose thermal resistance of

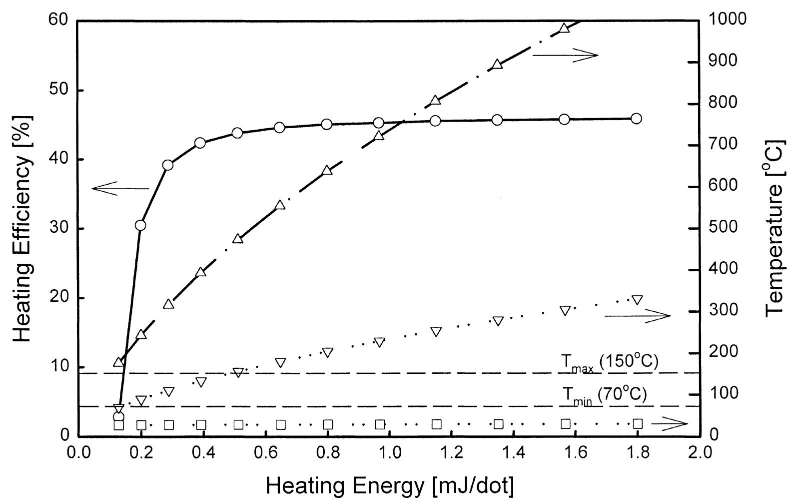

Fig. 12. The heating efficiency as function of bias energy with conditions t_d=2 ms, s_1=1 μm and G_s=10^5 W/°C. Blank circles (○) denote the heating efficiency, up triangles (△) denote the maximum heater temperature, down triangles (▽) denote the maximum paper temperature, and squares (□) denote the substrate temperature.

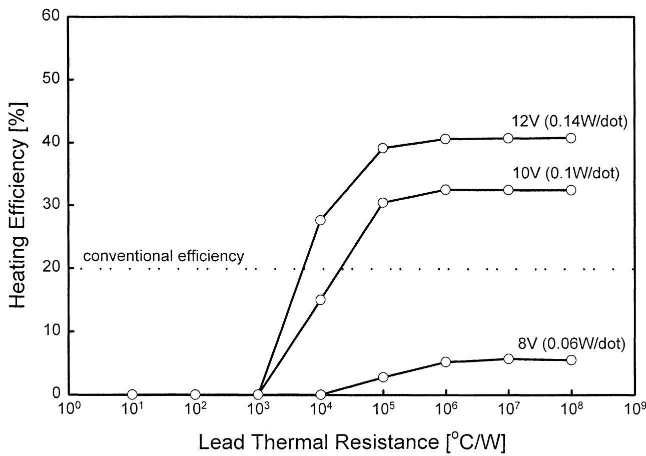

Fig. 13. Dependence of the heating efficiency on the solid thermal resistance with conditions: t_d=2 ms and s_1=1 μm.

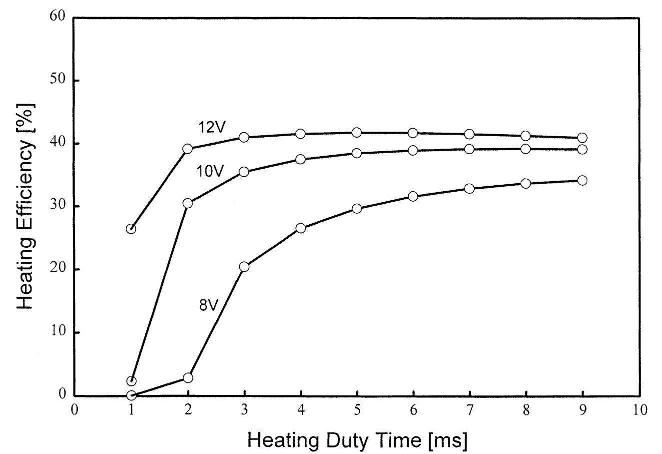

Fig. 14. The heating efficiency as function of heating duty time with conditions: s_1=1 μm and G_s=10^5 W/°C.

10^4 °C/W, a value which can be achieved easily by micromachined floating structures [19].

The efficiency can be improved by increasing the heating duty and instantaneous power. This is shown in Fig. 14: a higher power or a longer duty cycle sustains a longer effective printing time in the blackening temperature regime, hence is more efficient. For 10 V bias and when the duty time is below 2 ms, the efficiency drops quickly in our simulated device. However, this deterioration phenomenon can be reduced if the bias voltage is increased.

The air gap is the most important factor to the proposed contact-less thermal printing. All simulations indicate the efficiency is nearly inversely proportional to the air gap as that shown in Fig. 15. This is consistent with Eq. (3). Although more than 50% efficiency can be achieved by a shallow 0.2 μm spacing, in practice, holding such a spacing is difficult due to the roughness of thermal marking paper [2] and other machinery precision. A total of 1 μm spacing or more is practical, which can provide approximately a 40% efficiency with 12 V supply voltage (solid dot in Fig. 15). Under this condition, the paper's temperature falls to the middle of T_{max} and T_{min}, while the heater's temperature is below 350°C, both are appropriated.

Table 3 summarizes the present studies with the data collected from other reports. Case A is illustrated for maximum efficiency. In this case, a highest efficiency of 42% can be achieved with a median printing speed. However, higher power should be applied resulting in higher heater temperature rise to 393°C. This temperature is safe, because the highly pure thermal oxide of silicon on the top of the microheater is reported having a glass transition temperature up to 1600°C [21]. Case B is calculated for minimum printing power. In such case, the peak power required is only 60 mW per pixel, a quantity much lower than that reported by Mitsubishi Company and Sanders (columns 1 and 2). The low power demand is simply due to the longer heating duty as explained before. Case C is calculated for maximum printing speed. Our study reveals that, even in very high

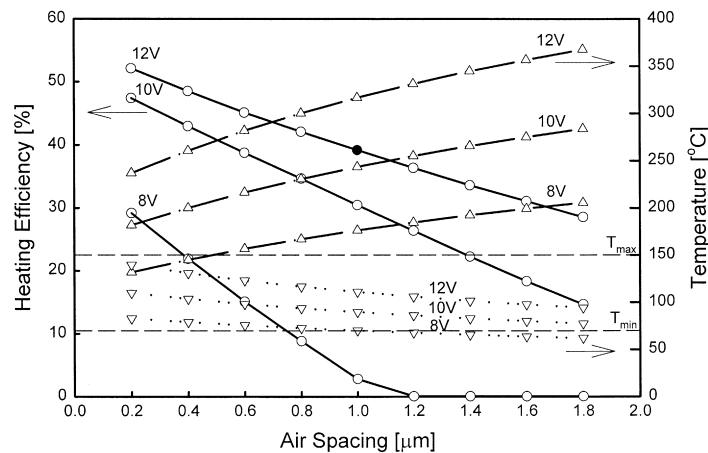

Fig. 15. The heating efficiency and associated temperature as functions of air gap with the conditions: t_d=2 ms, s_1=1 μm, G_s=10^5 W/°C. The symbols used here are identical to that in Fig. 12.

Table 3
Comparison of thermal printing performances of various studies

	Mitsubishi Co.[a]	Sanders[b]	Mochizuki[c]	This study		
				Case A	Case B	Case C
Resolution (dpi)	200	200	140	200	200	200
Ambient temperature (°C)	25	20	20	27	27	27
Substrate temperature (°C)	65	70	50	28.1	27.6	27.8
Max. heater temperature (°C)	300	300	210	393	218	301
Heating energy (mJ/dot)	0.45	0.3	–	0.4	0.54	0.14
Applied power (W/dot)	0.45	0.3	–	0.2	0.06	0.14
Applied duty time (ms)	1	1	0.1	2	9	1
Printing speed (ms/line)	10	10	2	2.5	10	1.5
(ppm) (A4-size)	4	4	28	16	4	27
Heating efficiency (%)	20	–	–	42	34	26

[a] [3].
[b] Thermal transfer printing case [18].
[c] [20].

speed printing of 27 ppm (Case C), the 26% efficiency is still higher than the conventional 20% (Column 1). Interestingly, the heating energy is also considerably saving because of the paper temperature is heated closely above the minimum blacken temperature of 70°C. In all cases, the substrate temperature rising above the ambient is uniquely low with this device.

In summary, the above extensive simulations indicate positively that the micromachined resistive heater and its structure can be used as an effective contact-less, thermally marking element.

In future design, a structure with extended thin glass fin aside the micro-heater so that most of the v-groove area can be covered should be considered for having not only larger gas contact area, but also better graphic modulation transfer function (MTF) [22].

5. Conclusion

The method utilizing a micromachined resistive heater array for contact-less DTP has been described and analyzed by electrothermal SPICE simulation. The study indicates that this new device is not only feasible, its performances are also superior to the conventional thick-film or thin-film devices due to its miniature thermal mass and excellent thermal isolation from the substrate. The new microfabrication process allows the heater array and the related driving circuits being monolithically integrated on the same chip, which is expectably cost-effective.

References

[1] K. McConnell, D. Bodson, S. Urban, Fax: Facsimile Technology and Systems, 3rd Edition, Artech House, Boston, 1999, pp. 141–157.
[2] J.J. Johnson, Principles of Non-Impact Printing, Palatino Press, USA, 1986, Chapter 5, pp. 164–175.
[3] Mitsubishi Thermal Head: Technical Guide, Mitsubishi Electric Co., Tokyo, 1987, pp. 1–48.
[4] M. von Smoluchowski, Ann. Physik 35 (1911) 983.
[5] S. Dushman, Scientific Foundations of Vacuum Technique, 2nd Edition, Wiley, New York, 1962, Chapter 1, pp. 39–53.
[6] A.W. van Herwaarden, P.M. Sarro, Double-beam integrated thermal vacuum sensor, J. Vac. Sci. Technol. A5 (1987) 2454–2457.
[7] W. Lang, Heat transport from a chip, IEEE Trans. Electron Devices ED-37 (1990) 958–963.
[8] F.P. Incropera, D.P. DeWitt, Fundamentals of Heat and Mass Transfer, 3rd Edition, Wiley, New York, 1990, Chapter 7, pp. 389–400.
[9] R.H. Kingston, Detection of Optical and Infrared Radiation, Springer, New York, 1978, Chapter 7, pp. 89–93.
[10] F.P. Incropera, D.P. DeWitt, Fundamentals of Heat and Mass Transfer, 3rd Edition, Wiley, New York, 1990, Appendix A.
[11] A. Bohg, Ethylene diamine–pyrocatechol–water mixture shows etching anomaly in boron-doped silicon, J. Electrochem. Soc. 118 (1971) 401–402.
[12] P.K. Weng, J.S. Shie, Micro-Pirani vacuum gauge, Rev. Sci. Instrum. 65 (1994) 492–499.
[13] N.R. Swart, A. Nathan, Flow-rate microsensor modelling and optimization using SPICE, Sens. Actuators A34 (1992) 109–122.
[14] F.J. Auerbach, G. Meiendres, R. Muller, G.J.E. Scheller, Simulation of the thermal behavior of thermal flow sensors by equivalent electrical circuits, Sens. Actuators A41–42 (1994) 275–278.
[15] J.S. Shie, Y.M. Chen, M. Ou-Yang, C.S. Chou, Characterization and modeling of metal-film microbolometer, J. Microelectromech. Syst. 5 (1996) 298–306.
[16] C.S. Chou, Y.M. Chen, M. Ou-Yang, J.S. Shie, A sensitive Pirani vacuum sensor and the electrothermal SPICE modeling, Sens. Actuators A53 (1996) 273–277.
[17] N.R. Swart, A.N. Nathan, Coupled electrothermal modeling of microheaters using SPICE, IEEE Trans. Electron Devices ED-41 (1994) 920-925.
[18] D.J. Sanders, Heat conduction in thermal transfer printing, Can. J. Chem. 63 (1985) 184–188.
[19] Y.M. Chen, J.S. Shie, Thunter Hwang, Parameter extraction of resistive thermal sensors, Sens. Actuators A55 (1996) 43–47.
[20] S. Mochizuki, Y. Kudoh, T. Tsukada, The effect of heat transfer process on the print quality in thermal printers, JSME Int. J. 31 (1988) 553–558.
[21] S.M. Sze, Physics of Semiconductor Devices, 2nd Edition, Wiley, New York, 1981.
[22] J.W. Goodman, Introduction to Fourier Optics, McGraw-Hill, 1968, Chapter 6, pp. 101–140.

Biographies

Yeong-Maw Chen received his BSc degree in physics from National Central University of Taiwan in 1981, and his master degree in electro-optical engineering from National Chiao Tung University in 1983. Since then he has been working in CSIST on microwave system design. He is currently a PhD candidate in the Institute of Electro-Optical Engineering of National Chiao Tung University, majoring in thermal printing technology.

Dr. Jin-Shown Shie currently is the President of Integrated Crystal Technology Corporation, the company he found recently devoting to integrated micro-sensor fabrication. He has retired in August 1999 as an emeritus professor from the Institute of Electro-Optical Engineering at National Chiao Tung University, where he had taught since 1973. Before, he received a PhD degree from the Department of Materials Science at SUNY Stony Brook, USA, 1972, and earned in Taiwan a MSEE degree in 1968 and a BSEE degree in 1965 from National Chiao Tung University and National Cheng Kung University, respectively. His current research is focused on uncooled thermal sensors.